PERGAMON

Vision Research 39 (1999) 207–217

Vision Research

Off-axis monochromatic aberrations estimated from double pass measurements in the human eye

Antonio Guirao, Pablo Artal *

Laboratorio de Optica, Departamento de Física, Universidad de Murcia, Campus de Espinardo (Edificio C), 30071 Murcia, Spain

Received 4 August 1997; received in revised form 24 April 1998

Abstract

Off-axis monochromatic aberrations in the human eye impose limits on peripheral vision. However, the magnitude of the aberrations off-axis, and in particular coma, has not been yet completely determined. We have developed a procedure to estimate third order aberrations in the periphery of the human eye. The technique is based on recording series of double pass retinal images with unequal entrance and exit pupil diameters (Artal, Iglesias, López-Gil & Green (1995b). *J. Opt. Soc. Am. A*, *12*, 2358–2366.) which allows the odd asymmetries in the retinal image be assessed. The procedure that is described provides accurate estimates of the main off-axis aberrations: astigmatism, defocus and coma. We have measured these aberrations in four normal subjects. For a given eccentricity, the measured amount of coma and astigmatism are relatively similar among subjects, because the angular distance from the axis is the dominant factor in determining the magnitude of these aberrations. However, we found considerable variability in the values of peripheral defocus, probably due to a complicate combination of off-axis aberrations and fundus shape. The final off-axis optical performance of the eye for a given object location is determined by a particular mixture of defocus, astigmatism, coma and higher order aberrations.

Keywords: Optical aberrations; Peripheral vision; Refraction; Astigmatism; Human eye

1. Introduction

Although aberrations greatly increase for objects located off-axis, the peripheral image quality in the human eye has not been as well studied as the optical performance in the fovea. Previous work has concentrated on off-axis refraction, including oblique astigmatism (Ferree & Rand, 1933; Rempt, Hoogerheide & Hoogenboom, 1971; Lotmar & Lotmar, 1974; Millodot & Lamont, 1974; Smith & Lu, 1991), on the effect of refractive errors on spatial resolution, motion or retinal undersampling (aliasing) in the periphery (Banks, Sekuler & Anderson, 1991; Anderson, Mullen & Hess, 1991; Artal, Derrington & Colombo, 1995a; Galvin, Williams & Coletta, 1996; Thibos, Still & Bradley, 1996; Wang, Thibos & Bradley, 1997) and on the off-axis modulation transfer function (MTF) obtained with the double pass method (Jennings & Charman, 1981; Navarro, Artal & Williams, 1993). However, the characteristics of the aberrations, in particular coma, in the periphery has not been yet completely determined.

Röhler (1962) obtained the first estimates of the modulation transfer at some spatial frequencies in the periphery by using an ophthalmoscopic method. Jennings & Charman (1981) obtained the line spread function (LSF) as a function of the eccentricity () and more recently, Navarro, Artal & Williams (1993) using the double pass apparatus of Santamaría, Artal & Bescós (1987) obtained a map of double pass retinal images and the average MTFs for a wide peripheral area (− 60–60°) in the horizontal meridian. The double pass images were collected with natural accommodation and the foveal spherical refractive correction. Williams, Artal, Navarro, McMahon, & Brainard (1996) recorded double pass images after correction of focus and astigmatism for every eccentricity. Jennings & Charman (1997) studied how different analytical expressions represent the experimental off-axis MTFs. All these results showed a decay in the optical image quality with the eccentricity that did not account completely for the decline in visual resolution one finds in the periphery.

* Corresponding author. Fax: + 34 968 363528; e-mail: pablo@fcu.um.es.

0042-6989/98/$ - see front matter
PII: S0042-6989(98)00159-X

Table 1
The first nine Zernike polynomials and their interpretation in Seidel aberrations

Zernike polynomials	Interpretation
$Z_1 = 1$	Constant
$Z_2 = 2\rho \cos\theta$	Tilt
$Z_3 = 2\rho \sin\theta$	Tilt
$Z_4 = \sqrt{3}(2\rho^2-1)$	Defocus
$Z_5 = \sqrt{6}\,\rho^2 \cos 2\theta$	Astigmatism
$Z_6 = \sqrt{6}\,\rho^2 \sin 2\theta$	Astigmatism
$Z_7 = \sqrt{8}(3\rho^2-2)\rho \cos\theta$	Coma and tilt
$Z_8 = \sqrt{8}(3\rho^2-2)\rho \sin\theta$	Coma and tilt
$Z_9 = \sqrt{5}(6\rho^4-6\rho^2+1)$	Spherical and defocus

Astigmatism and defocus are usually assumed to be the main aberrations off-axis in the human eye, but the contribution of coma off-axis has not been specifically studied. One reason is that in the double pass images, recorded with equal pupil diameters, coma-like aberrations appear as symmetrical aberrations (Artal, Marcos, Navarro & Williams, 1995c). The purpose of this work is to estimate the relative contribution of monochromatic off-axis aberrations, with special emphasis in defocus, astigmatism and coma, using a new version of the double pass apparatus that uses unequal pupils (Artal, Iglesias, López-Gil & Green, 1995b).

2. Methods

2.1. Theory

In this paper we will only consider third order, or Seidel, aberrations, which is a reasonable approximation for aperture diameters less than 4 mm, although at large eccentricities (45°), fourth and higher order aberrations could also be important. The wave aberration function is defined as the optical deviation of the wavefront along a certain ray from the gaussian spherical wavefront (Born & Wolf, 1985). The wave aberration can be expressed in terms of a Seidel expansion by

$$W(p,\theta) = A_t\rho\cos\theta + A_d\rho^2 + A_a\rho^2\cos^2\theta + A_c\rho^3\cos\theta + A_s\rho^4 \quad (1)$$

with (ρ, θ) polar coordinates over the exit pupil, ρ normalized to one, and A_t, A_d, A_a, A_c, A_s represents units of length corresponding to tilt, defocus, astigmatism, coma and spherical aberration coefficients respectively. The coefficients of astigmatism (A_a) and coma (A_c) in Eq. (1) for off-axis point objects at infinity in a spherical surface, with a circular pupil, can be expressed by

$$A_a = \frac{n^2}{2n'}\frac{r_0^2}{f'}\sin^2\omega; \qquad A_c = \frac{n^2}{4n'}\frac{r_0^3}{Rf'}\sin^2\omega; \quad (2)$$

where f' is the focal distance, n, n' are the refractive indexes, ω is the eccentricity angle, R is the curvature

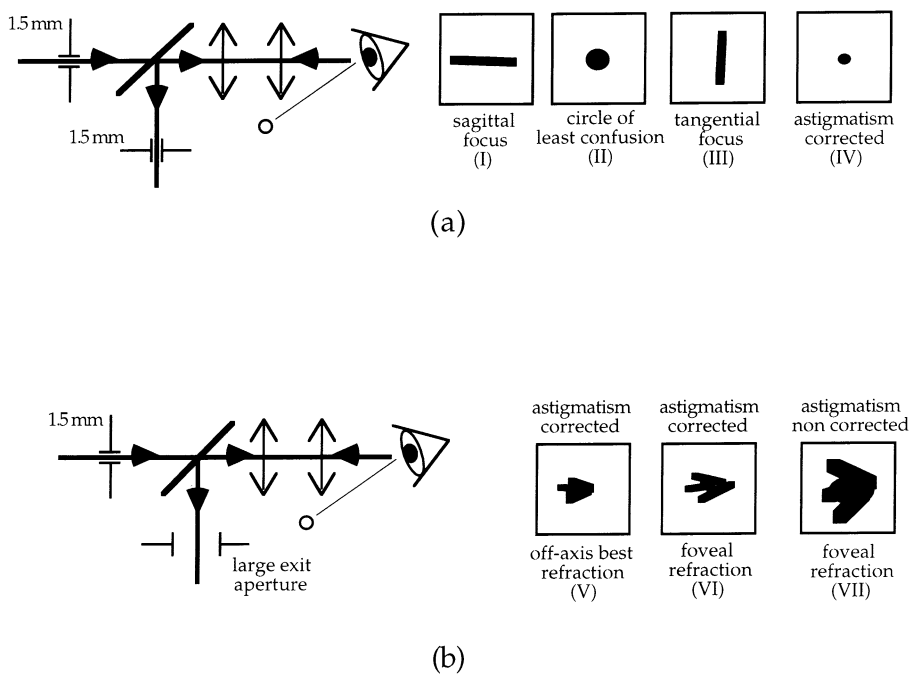

Fig. 1. Schematic diagram of the procedure, showing the type of double pass images recorded in each subject for every eccentricity. Panel (a) illustrates the experimental configuration with small equal pupils in both passages (1.5–1.5 mm). Three images at different focus positions (I, II, III) are recorded to determine the Sturm interval. Another image (IV) is recorded with the appropriate cylindrical lens to correct the estimated astigmatism. Panel (b) shows the second series of measurements. In this case, the entrance pupil diameter is keep 1.5 mm diameter and the exit pupil is the natural pupil (around 4 mm diameter). Three types of double pass images (V, VI, VII) were recorded to evaluate the different contribution of each aberration (see the text for further details).

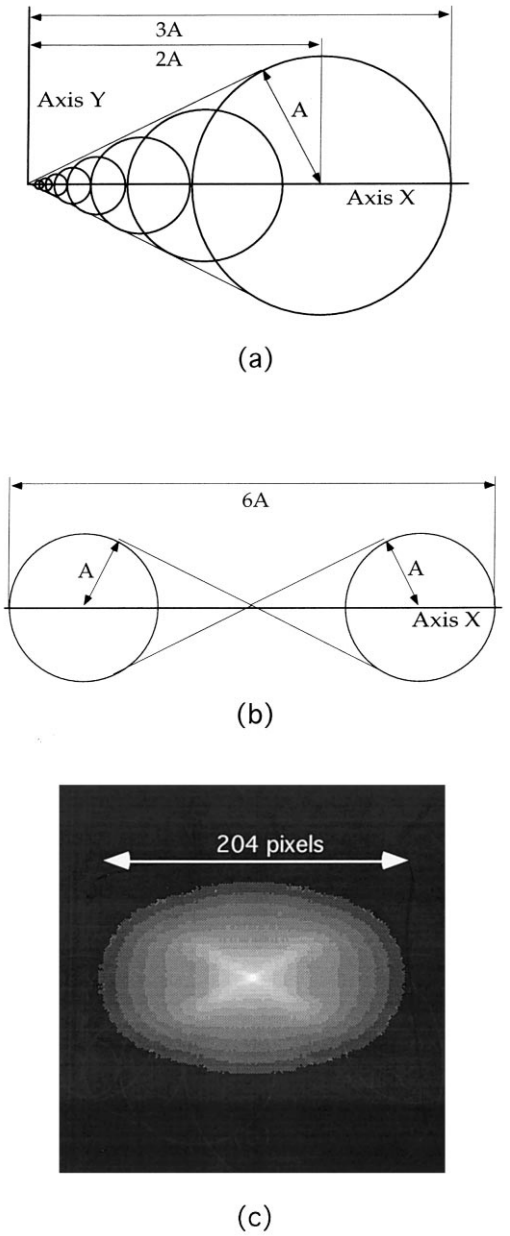

Fig. 2. (a) Schematic diagram of the typical shape of a PSF affected by a pure coma aberration. The size of the image is related to the value of the coma coefficient. (b) Schematic diagram of the correlation of two PSFs affected by coma (double pass image). The horizontal extension (6A) is in relation with the amount of coma. (c) Double pass image corresponding to a simulated eye affected only by third order coma. (Additional details are in the text).

radius of the surface and r_0 is the exit pupil's radius. These expressions were obtained in a similar way as described in Mahajan (1991) but without using the small angles approximation. The coefficient of astigmatism depends on the first power of r_0/f', while coma depends on $(r_0/f')^2$. This means that for small pupil diameters, astigmatism is dominant. On the other hand, since coma depends on the eccentricity angle through $\sin 2\omega$, while the astigmatism depends through $\sin^2 \omega$, for small eccentricity angles, coma is comparatively larger than astigmatism.

An alternative way to describe the wave aberration is by means of the Zernike polynomials expansion (Born & Wolf, 1985). Table 1 presents the third order Zernike polynomials. Since our measurements are obtained in the horizontal meridian (XZ plane), astigmatism and coma are along the X axis, and only terms Z_5 and Z_7 are required. The relationship between Seidel (Eq. (1)) and Zernike (Table 1) coefficients is given by:

$$A_d = 2\sqrt{3}\, a_4 - 6\sqrt{5}\, a_9 - \sqrt{6}\, a_5,$$
$$A_a = 2\sqrt{6}\, a_5,$$
$$A_c = 3\sqrt{8}\, a_7,$$
$$A_s = 6\sqrt{5}\, a_9, \quad (3)$$

2.2. Experimental procedure

We used a double-pass apparatus (Santamaría, Artal & Bescós, 1987) similar to others previously applied for experiments in the periphery (Navarro, Artal & Williams, 1993; Williams, Artal, Navarro, McMahon & Brainard, 1996), but incorporating different size entrance and exit apertures (Artal et al., 1995b). This permits recording of double pass images that keep information on the odd aberrations. The light source was a He-Ne laser (543 nm) and the fixation target a green LED located at optical infinity and viewed through a mirror to select the desired retinal eccentricities (15, 30 and 45°) in the temporal horizontal meridian. Double-pass images (4 s-exposure) were recorded with a scientific grade cooled CCD camera (Compuscope CCD 800) and digitized to 256×256 pixels (that corresponds to a field of view of 80 min of arc) with 12 bits/pixel.

The measurements were carried out in the right eye of four normal male subjects: AN (25 years old, 1.5 D myopic, nearly astigmatism free); FV (25 years old, 1 D myopic, no astigmatism); NN (23 years old, 3 D myopic, -0.75 of astigmatism at 60°); PA (35 years old, 2.5 D myopic, no astigmatism). The subjects fixated at the LED test located around their remote point without paralyzing the accommodation. In every subject, we recorded two series of double pass images at each eccentricity, as schematically described in Fig. 1(a, b), with an entrance diameter of 1.5 mm and exit aperture diameter either of 1.5 mm or the eye's natural pupil (with a diameter around 4 mm, measured by an infrared pupil-meter). With the first series of measurements using equal 1.5 mm diameter pupil in both passes, we determined the amount of astigmatism (Fig. 1a). We changed the focus to record double pass images that corresponds to the extremes of the Sturm interval: sagittal (I) and tangential (III) foci, and the least confu-

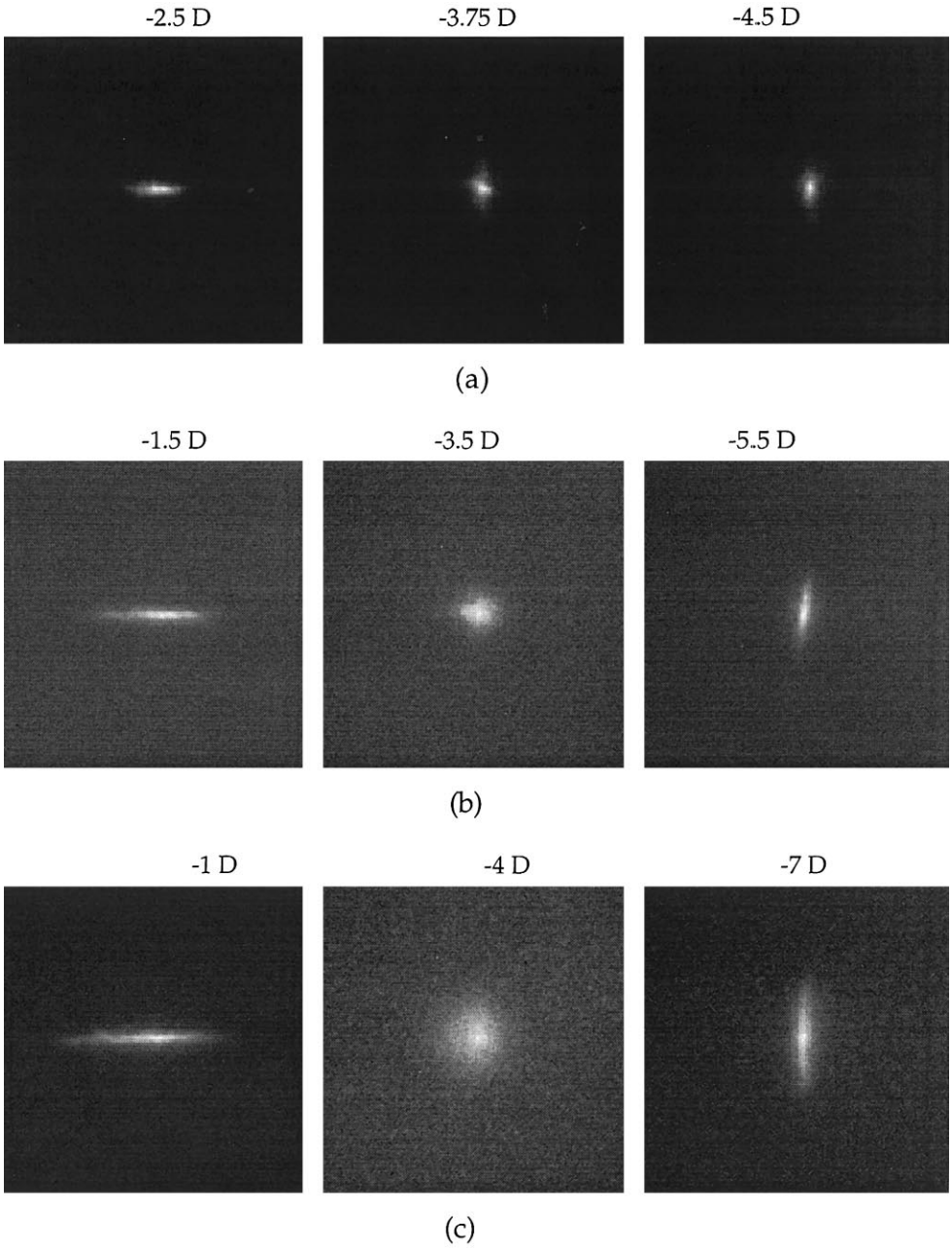

Fig. 3. Double-pass images obtained with 1.5–1.5 mm artificial pupils corresponding to the images type I, II, III in Fig. 1 (a) at 15 (a), 30 (b) and 45° (c) of eccentricity in subject NN. The number in diopters appearing in each image refers to the refractive position. Each image subtends 80 min of arc.

sion circle (II). An additional double pass image was recorded with the astigmatism corrected (IV) by placing the appropriate cylindrical lens for the sagittal focus. If image (IV) was not elongated and was more compact than the image of type II (the least confusion circle), we concluded that astigmatism was corrected. In the second series of measurements (Fig. 1b), we recorded three different double pass images using the unequal diameter aperture configuration (1.5–4 mm):

(V) At the sagittal off-axis focus with the appropriate cylindrical lens to correct astigmatism. This image reveals all the existing aberrations except astigmatism and defocus. We expect that coma will be the main relevant aberration remaining in this image.

(VI) With the astigmatism still corrected but with the spherical refraction corresponding to foveal vision

(VII) With the foveal refraction and the astigmatism not corrected (without the cylindrical lens). This image corresponds to the actual retinal image in the periphery for an object located at infinity and includes all the existing aberrations off-axis.

Table 2
Experimental values of astigmatism for each subject and eccentricity expressed in diopters, and the mean value of Zernike coefficient a_5 in number of wavelengths for 1.5 and 4 mm pupil diameter

ω (°)	Astigmatim (diopters)					Mean a_5 (in λ)	
	PA	FV	AN	NN	Mean	1.5 mm	4 mm
15	1	1.75	1	2	1.44	0.17	1.21
30	2.5	2.5	1.5	3.5	2.50	0.29	2.06
45	5	5	4.5	6	5.12	0.59	4.19

By comparison of images (V), (VI) and (VII), the different contributions of defocus, astigmatism and coma to the off-axis retinal image are evaluated.

2.3. Estimation of the amount of coma from double pass images

We developed a procedure to estimate the amount of coma from the geometry of the double pass images. This is based in the analysis of the typical shape of the double pass images produced by a system with coma. The ray spot diagram on the image plane corresponding to a system with only coma aberration is given by (Mahajan, 91):

$$\begin{cases} x = A\rho^2(2+\cos 2\theta) \\ y = A\rho^2 \sin 2\theta \end{cases} \quad ; \; A \equiv A_c\frac{f'}{r_0} \tag{4}$$

with (ρ, θ) being polar coordinates, A_c the coefficient of coma, f' the focal length of the system and r_0 the pupil radius. Eq. (4) represents a series of parametric circumferences with center in $(2A\rho^2, 0)$ and radio $A\rho^2$. The point-spread function (PSF) is the superposition of the infinite circumferences obtained when ρ cover the interval (0, 1) over the normalized pupil. The maximum extension of the PSF is $3A$ along the X axis and $2A$ along Y (Fig. 2a). On the other hand, the double pass image is the convolution of the PSFs corresponding to the first and the second passes (Artal, Marcos, Navarro & Williams, 1995c). For the double pass configuration with equal pupil diameters in the entrance and exit pupils, the double pass image is the autocorrelation of the PSF. For a system with only coma, the double pass image, shown schematically in Fig. 2(b), has an extension along the X axis of $6A$.

We obtained an estimation of the coma coefficient from the extension of the double pass images recorded with equal pupil diameter (1.5 mm) when defocus and astigmatism were corrected (images type IV in Fig. 1a). If we assume that the impact of other aberrations in these images is rather limited due to the small pupil diameters used (1.5 mm), coma should play the major role to enlarge these double pass images (type IV). The relationship between the spread of these images (in number of pixels) and the coefficient of coma (a_7 in the Zernike polynomials expansion), when the wavelength

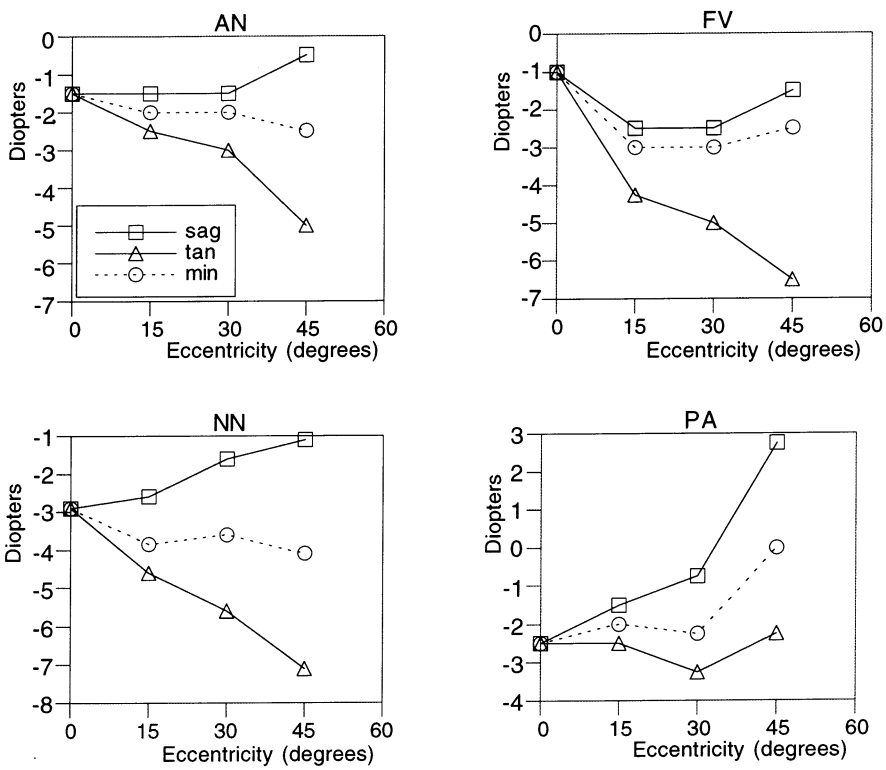

Fig. 4. Refractive positions for the tangential (tan) and sagittal (sag) foci and the circle of least confusion (min) at each eccentricity. One diagram for each subject (AN, FV, NN, PA). Negative values indicate myopia.

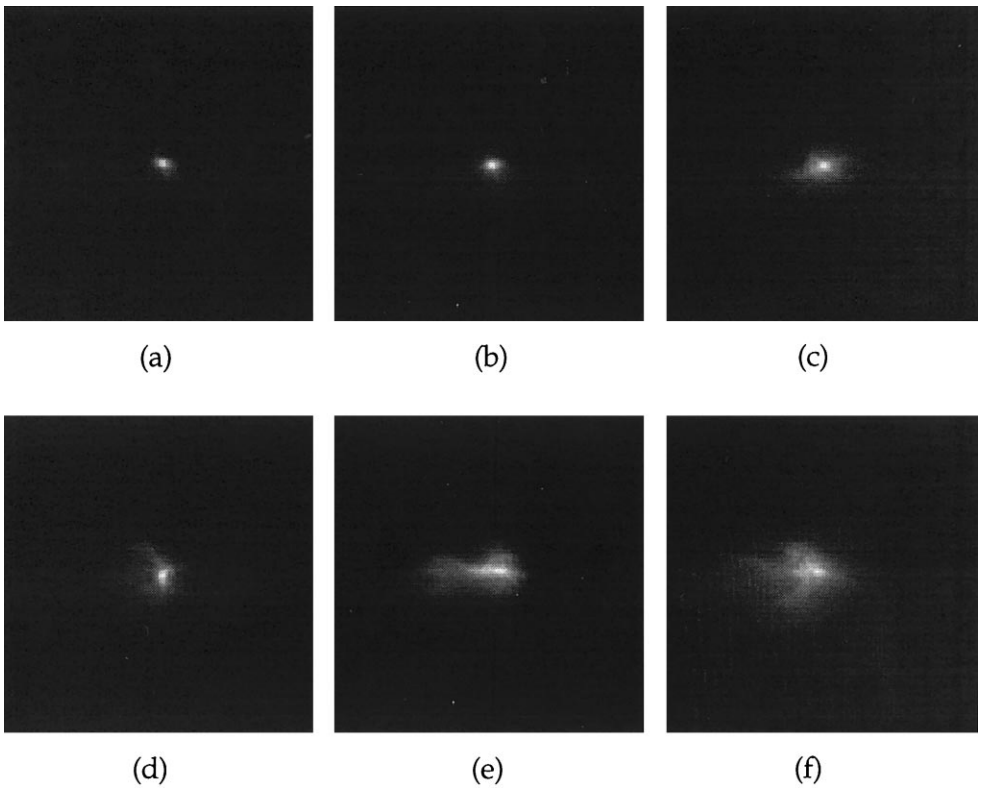

Fig. 5. Double-pass images recorded with astigmatism and defocus corrected, 1.5-1.5 mm (images type IV), for subject FV. (a) 15°, −1.5 D focus, −1.75 D astigmatism. (b) 30°, −1.5 D focus, −2.5 D astigmatism. (c) 45°, −0.5 D focus, −5 D astigmatism. With 1.5–4 mm pupil diameter (configuration V) for subject PA. (d) 15°, +1 D focus, −1 D astigmatism. (e) 30°, +1.75 D focus, −2.5 D astigmatism. (f) 45°, +5.25 D focus, −5 D astigmatism. Each image subtends 80 min of arc.

($\lambda = 543$ nm), the magnification in the set-up and the size of the pixel on the CCD camera are considered, is given by the equation:

$$A = 51.2 \cdot \frac{a_7(\text{in } \lambda)}{r_0(\text{in mm})} \text{ pixels.} \quad (5)$$

From the double pass images of type IV, we extracted the horizontal extension (6A) and subsequently the coma coefficient was calculated by Eq. (5). This coma coefficient (a_7) corresponds to a 1.5 mm diameter pupil ($r_0 = 0.75$ mm). The value of the coma coefficient for other pupil diameters was obtained by normalization (i.e.; for 4 mm pupil diameter multiplying by the factor $(4/1.5)^3$). Fig. 2(c) shows an example of the procedure in a computer simulated image. The grey level image is the autocorrelation of the PSF corresponding to a system with a pure coma aberration ($a_7 = 0.5\lambda$) for a 1.5 mm diameter pupil, with an horizontal spread ($6A$) of 204 pixels. By applying Eq. (5), we obtained the correct value of the coma coefficient.

Table 3
Experimental values of coma for each subject and eccentricity. The absolute value of the coefficient (a_7) is shown (the actual value are negative)

	Zernike coefficient, $\lvert a_7 \rvert$ (in λ)				1.5 mm	4 mm
w	PA	FV	AN	NN	Mean	Mean
15°	0.083	0.081	0.076	0.090	0.083	1.574
30°	0.105	0.107	0.110	0.122	0.111	2.104
45°	0.149	0.158	0.137	0.156	0.150	2.844

From 1.5 to 4 mm pupil diameter there are a multiplicative factor of $(4/1.5)^3$.

3. Results

3.1. Astigmatism

Fig. 3 shows the double pass images obtained for subject NN at 15, 30 and 45° of eccentricity with 1.5 mm diameter exit and entrance pupils (experimental configuration of Fig. 1a). At each retinal eccentricity, we recorded the images corresponding to the sagittal and tangential foci, and the circle of least confusion. For the others three subjects participating in the study, the same series of images were recorded. From the

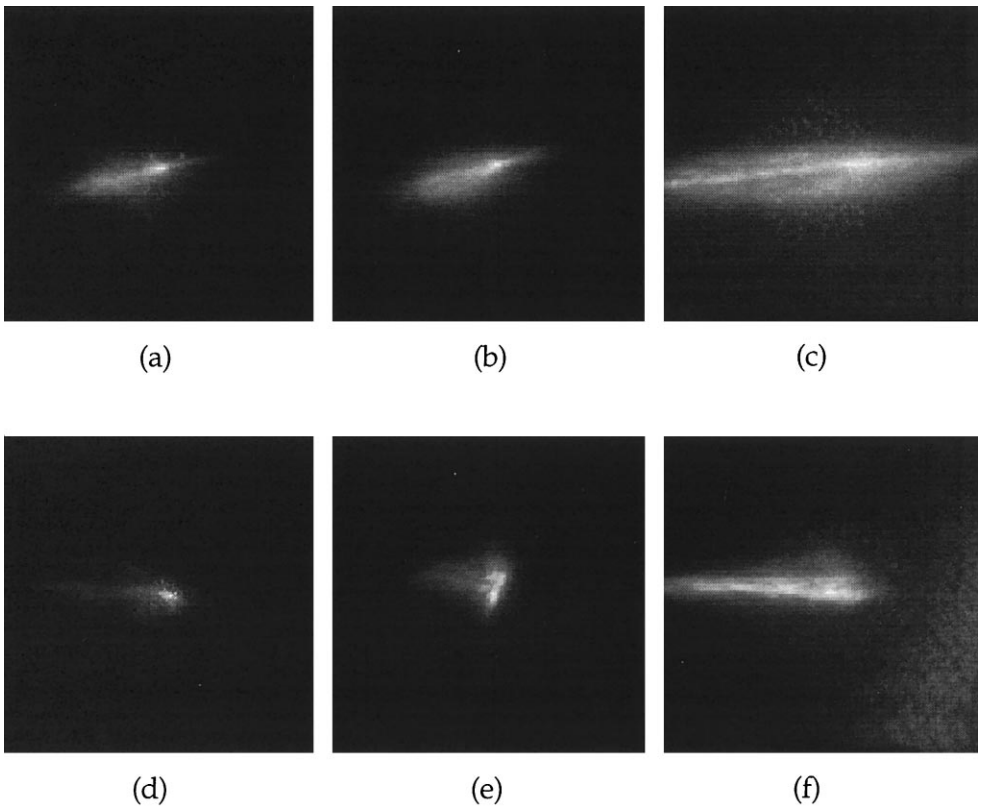

Fig. 6. Double-pass images with 1.5–4 mm for two subjects. Panels a–c corresponds to subject FV at 45°. (a) Defocus (− 0.5 D) and astigmatism (− 5 D) corrected. (b) Only astigmatism (− 5 D) corrected. (c) All peripheral aberrations. Panels d-f corresponds to subject NN at 30°. (d) Defocus (+ 1.25 D) and astigmatism (− 3.5 D) corrected. (e) only astigmatism (− 3.5 D) corrected. (f) All peripheral aberrations.

focus settings, the Sturm interval (i.e. the amount of astigmatism) was estimated. Table 2 shows the results of astigmatism in diopters for each observer at each eccentricity and the value of the astigmatism in terms of the Zernike coefficient (a_5), expressed in number of wavelengths, for 1.5 and 4 mm pupil diameters. These results of oblique astigmatism are, in average, similar to those obtained in previous works (compiled by Smith & Lu (1991)). Fig. 4 presents diagrams, for each subject, of the refractive positions for the tangential and sagittal foci and the circle of least confusion at every retinal eccentricity and in the fovea. The circle of least confusion appears approximately in the center of the Sturm interval, except for subject FV, possibly due to the effect of other aberrations. Williams, Artal, Navarro, McMahon & Brainard (1996) obtained approximately the same results for subject PA (Fig. 4 in that reference). This subject (PA) becomes more hyperopic in the periphery, in particular for large eccentricities. However, subject FV tends to a peripheral myopia even for moderate eccentricities. In subjects NN and AN, the refractive correction required to bring the circle of least confusion in coincidence with the retina is similar for every eccentricity.

3.2. Coma

Fig. 5 shows examples of peripheral double pass images recorded with astigmatism and defocus corrected. Panels a–c are images for subject FV at 15 (a), 30 (b) and 45° (c) obtained with 1.5 mm diameter in the aperture and exit pupils (images type IV). In particular, the image of panel (c) appears similar in shape as the autocorrelation of a pure coma (this can be noted by comparing this image with Fig. 2c). Panels (d–f) are the images for subject PA at 15 (d), 30 (e) and 45° (f) with the astigmatism and defocus corrected and obtained with 1.5 mm diameter entrance and the natural size exit pupil around 4 mm (images type V). These images are the convolution of the 1.5 mm-PSF with the 4 mm-PSF. These images present a comatic shape, suggesting that when astigmatism and defocus are corrected, the dominant remaining aberration is coma. We applied the procedure described above to estimate the coefficient of coma from the images type IV. Table 3 presents the absolute values of the Zernike coma coefficient (a_7) in number of wavelengths, for each subject and eccentricity. The average value for the four subjects at each eccentricity are given both for 1.5 and 4 mm diameter pupils.

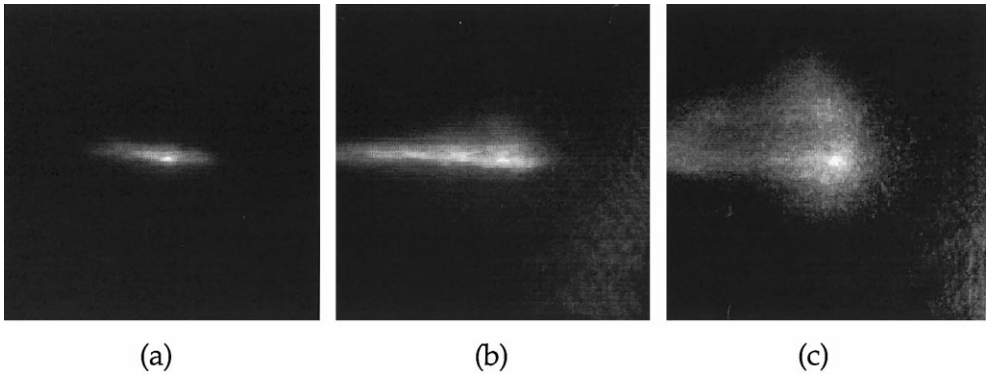

Fig. 7. Double-pass images with 1.5–4 mm for subject NN at each eccentricity without correction (all peripheral aberrations presents). (a) 15°, +0.5 D defocus, −2 D astigmatism; (b) 30°, +1.25 D defocus, −3.5 D astigmatism; (c) 45°, +1.75 D defocus, −6 D astigmatism.

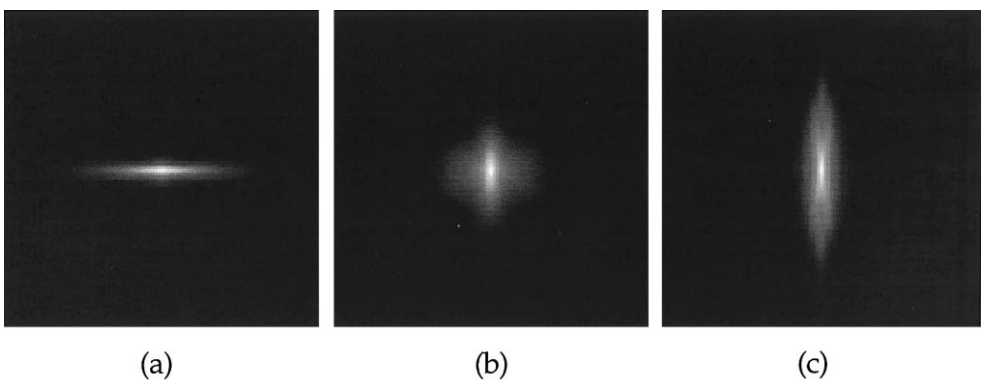

Fig. 8. Simulated double pass images (1.5–1.5 mm pupils) showing the peripheral astigmatism for subject NN at 45°. The images were calculated from the estimated coefficients of coma ($a_5 = 0.69\lambda$), astigmatism ($a_7 = -0.156\lambda$) and the different values of defocus (a) $a_4 = 0.49\lambda$; (b) $a_4 = 0$; (c) $a_4 = -0.49\lambda$.

Fig. 6 shows another sample of double pass images in the periphery in two subjects. Panels (a–c) are for subject FV at 45° of eccentricity and panels (d–f) for subject NN at 30°. The images were recorded under the conditions schematically described in Fig. 1 (b) (with 1.5 and 4 mm entrance and exit pupil diameter respectively). Panels (a) and (d) are the images with defocus and astigmatism corrected (images type V), panels (b) and (e) with the astigmatism corrected, but the foveal refraction (images type VI) and panels (c) and (f) with the foveal refraction and the astigmatism non corrected (images type VII). The comparison of the images (a) and (b) (or (d) and (e)) permits to evaluate the relative effect of defocus, while the comparison of the images (b) and (c) (or (e) and (f)) shows the relative effect of astigmatism. Fig. 7 shows three additional double pass images (at 15, 30 and 45°) obtained for subject NN with the foveal refraction and without correcting astigmatism. These images represent the off-axis performance at each eccentricity under normal viewing conditions for objects located at infinity.

3.3. Computer-generated double pass images

To further evaluate the procedure used to determine the amount of aberrations from the off-axis double pass images, we calculated the double pass images using the measured coefficients of astigmatism, coma and defocus. In this section, we present some examples of computer simulated double pass images to be compared with the experimentally recorded images. The results further confirm that those aberrations are dominant off-axis. As an example, Fig. 8 shows the simulated images for subject NN at 45° eccentricity for the sagittal (a), tangential (c) and circle of least confusion focus (b). The corresponding experimental images are in Fig. 3 (c). In this case, with the small pupil diameter (1.5 mm) and a large eccentricity (45°), both the simulated and real images are quite similar. Fig. 9 shows another example for subject PA at 30° (1.5 mm entrance pupil and 4 mm exit pupil). With the astigmatism corrected, we recorded double pass images at three different defocus: 0 D (a); −1 D (b) and −2 D (c). By using the estimated values of the aberrations, we obtained the

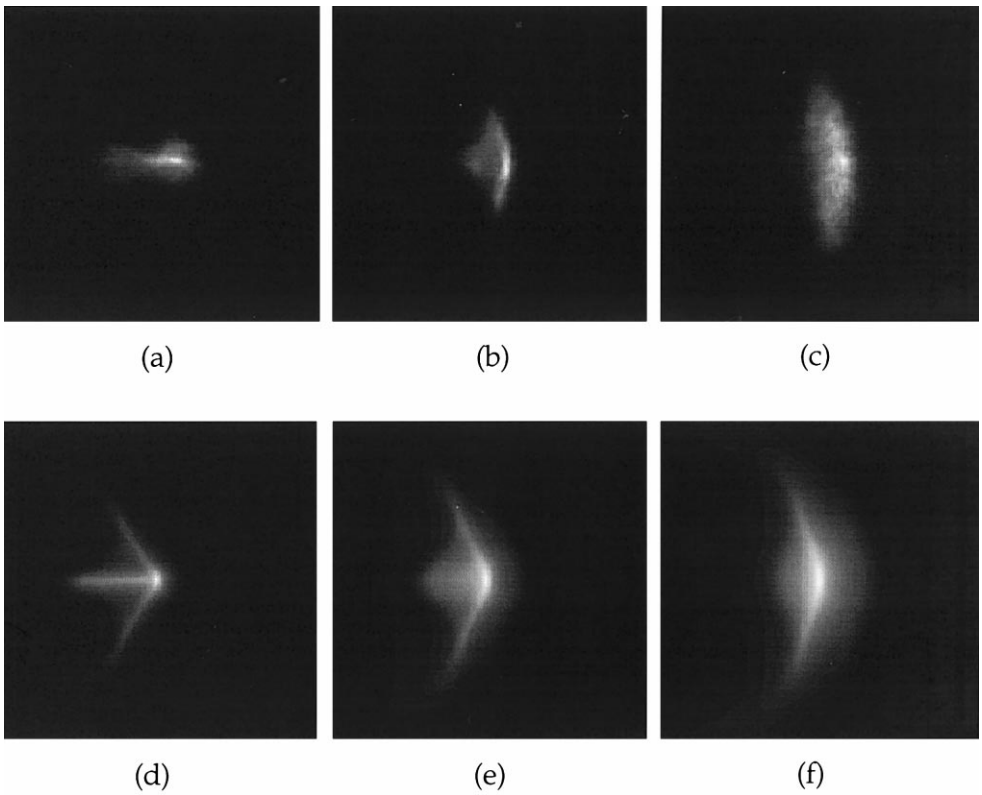

Fig. 9. Comparison among double-pass images for PA at 30° with 1.5–4 mm pupils and astigmatism corrected (a,b,c) and simulated images (d,e,f). Images shows the combination of coma with the defocus. Experimental double-pass images (-2.5 D astigmatism corrected) with the following defocus: (a) 0 D; (b) -1 D; (c) -2 D. Computer simulated images with the value coma coefficient ($a_7 = 0.105\lambda$) and different defocus; (d) $a_4 = 0\lambda$; (e) $a_4 = -0.16\lambda$; (f) $a_4 = -0.32\lambda$.

simulated images for each condition (d–f in Fig. 9). Although, there are differences between the two series of images due to noise and higher order aberration, the main spatial features in the images are approximately represented with these Seidel aberrations.

3.4. Off-axis 1.5 mm pupil diameter modulation transfer functions

For each subject and eccentricity, the MTF for 1.5 mm pupil diameter was calculated from the double pass images obtained with defocus and astigmatism corrected (images type IV). The mean one-dimensional radially averaged MTF for the four subjects and the three considered eccentricities are plotted in Fig. 10 (a), together with the diffraction-limited MTF for the same pupil diameter, included as a reference. Even for this small diameter pupil, and with astigmatism and defocus corrected, the MTFs were far from diffraction-limited. This is not surprising because, even in the fovea the MTFs for that pupil diameter were found to be not diffraction-limited (Artal, Marcos, Iglesias & Green, 1996). The decay of these MTFs with the eccentricity can be mainly attributed to the increasing coma with eccentricity and higher order aberrations. In part (b) of Fig. 10, the one-dimensional MTFs for 1.5 mm pupil diameter calculated from a pure coma aberration are shown. In particular, we used the mean values of the coma coefficient in the Zernike polynomial expansion ($a_7 = -0.083,\ -0.111,\ -0.15$ for 15, 30 and 45°, respectively). Although these MTFs are higher than the actual ones, because we only included coma, the relative drop in the MTFs is similar to that found in the experimental data, confirming than when astigmatism and defocus are corrected, coma remains as the main aberration.

3.5. Off-axis coma and astigmatism compared with predictions from a simple eye model

Fig. 11 (a) shows the measured values of the Zernike coefficient of coma (a_7) for 4 mm pupil diameter, expressed in number of wavelengths, for each subject and the eccentricities considered in this study. The solid line in the figure is the predicted value of coma as a function of the eccentricity using Eq. (2). This is the coma of a simple reduced eye model, just consisting in a single refractive spherical surface ($R = 5$ mm) separating two media of refractive indexes $n = 1$ and $n' = 4/3$. In Fig. 11 (b), the symbols represent the value of the measured astigmatism (Zernike coefficient (a_5)) for 4 mm pupil diameter, every subject and eccentricity. The

solid line is the theoretical prediction of astigmatism in the same reduced eye model. The simplest eye model (just one spherical surface) reproduces quite accurately the amount of coma with the eccentricity. However, the same model overestimate the amount of off-axis astigmatism. Recently an eye model consisting of one elliptical surface that reproduces the measured off-axis astigmatism was proposed (Wang & Thibos, 1997). Other more complicated eye models incorporating either aspherical surfaces (Lotmar, 1971; Lotmar & Lotmar, 1974) or a gradient index structure for the lens (Pomerantzeff, Pankratov, Wang & Dufault, 1984) have been also proposed to better account the off-axis astigmatism. The influence of the lens in the peripheral astigmatism was evaluated by measuring the off-axis astigmatism in pseudoaphakic eyes (Smith & Lu, 1991). In these patients, the values of off-axis astigmatism were larger than in normal subjects and closer to the theoretically predicted data with simple models.

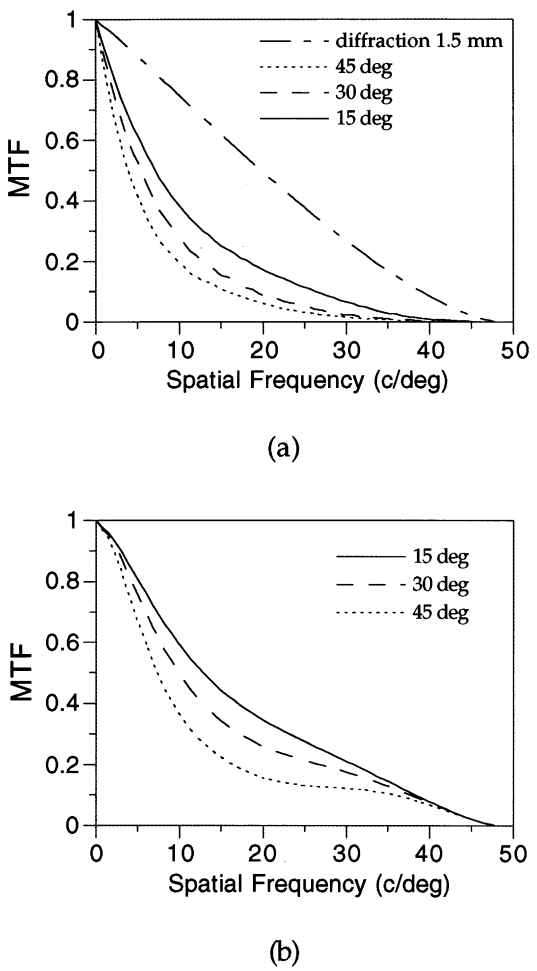

Fig. 10. MTFs for 1.5 mm at three retinal eccentricities. Each curve is the mean for the four subjects. (a) experimental MTF from double-pass images with 1.5–1.5 mm (astigmatism and defocus corrected). (b) theoretical MTF calculated from a pure coma wave-aberration (with mean coefficients of Table 3).

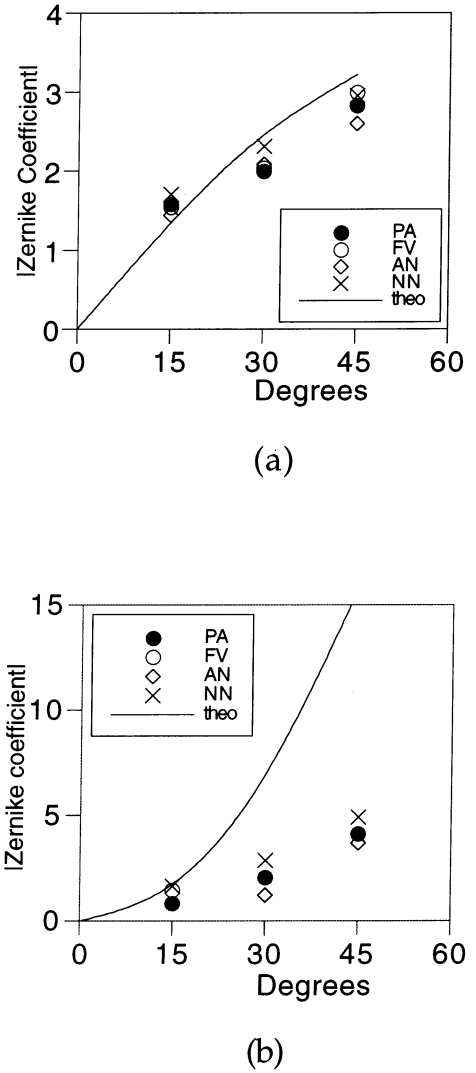

Fig. 11. Comparison of the values of coma (a) and astigmatism (b) as a function of the eccentricity predicted by a simple eye model and the estimated values in four subjects (see the text for further details).

4. Conclusions

In this paper, we presented results of the off-axis Seidel aberrations in four normal subjects. We extended the previous off-axis double pass measurements by incorporating in the setup the option of unequal entrance and exit pupil diameters (Artal, Iglesias, López-Gil & Green, 1995b). This procedure provides accurate data on the off-axis astigmatism, within the same range as those obtained in previous works. We also proposed a method to estimate the amount of coma from the double pass images obtained with small pupil diameters after correction of defocus and astigmatism. Astigmatism, coma and defocus were found to be the most important aberrations off-axis. The comparison of the computer-simulated double pass images with those recorded experimentally shows that the main features in shape and the overall size of the retinal images are

approximately described by these aberrations, although noise and higher order aberrations further complicate the particular shape of each image. The relative decay in the MTFs for 1.5 mm pupil diameter with the eccentricity, when defocus and astigmatism were corrected, can be mostly explained by the effect of the off-axis coma. At large eccentricities, the double pass images covers a large area of the retina even for small pupil diameters. For instance, at 45° at one of the astigmatic foci, the double pass image spread nearly one degree in the direction of maximum elongation. For objects located at infinity and large pupil diameters, the double pass images spread usually more than one degree. In normal visual conditions in white light, the effect of chromatic aberrations should be also considered. In particular, it has been suggested that lateral chromatic aberration plays a major role in further degrading the peripheral retinal image (Thibos, 1987). For a given eccentricity angle, the measured amount of coma and astigmatism were found to be relatively stable among subjects. The reason could be that the eccentricity angle is dominant in the functional dependence of these aberrations with eccentricity. However, we found a larger variability among subjects in the values of peripheral defocus. The final off-axis performance is produced by a particular mixture of defocus, astigmatism, coma and higher order aberrations.

Acknowledgements

This research was partially supported by a DGICYT grant n° PB94-1138-C02-01, Spain and by a grant from the Región de Murcia (Fundación Séneca). AG acknowledges a fellowship from CajaMurcia. We thank Ignacio Iglesias for help with some parts of software development and Daniel Green for a critical reading of the manuscript.

References

Anderson, S. J., Mullen, K. T., & Hess, R. F. (1991). Human peripheral spatial resolution for achromatic and chromatic stimuli: limits imposed by optical and retinal factors. *Journal of Physiology*, *442*, 47–64.

Artal, P., Derrington, A. M., & Colombo, E. (1995a). Refraction, aliasing, and the absence of motion reversals in peripheral vision. *Vision Research*, *35*, 939–947.

Artal, P., Iglesias, I., López-Gil, N., & Green, D. (1995b). Double-pass measurements of the retinal-image quality with unequal entrance and exit pupil sizes and the reversibility of the eye's optical system. *Journal of the Optical Society of America*, *A12*, 2358–2366.

Artal, P., Marcos, S., Navarro, R., & Williams, D. R. (1995c). Odd aberrations and double-pass measurements of retinal image quality. *Journal of the Optical Society of America*, *A12*, 195–201.

Artal, P., Marcos, S., Iglesias, I., & Green, D. G. (1996). Optical modulation transfer function and contrast sensitivity with decentered small pupils in the human eye. *Vision Research*, *36*, 3575–3586.

Banks, M. S., Sekuler, A. B., & Anderson, S. J. (1991). Peripheral spatial vision: limits imposed by optics, photoreceptors, and receptor pooling. *Journal of the Optical Society of America*, *A8*, 1775–1797.

Born, M., & Wolf, E. (1985). *Principles of optics*. New York, NY: Pergamon.

Ferree, C. E., & Rand, G. (1933). Interpretation of refractive conditions in the peripheral field of vision: a further study. *Archives of Ophthalmology*, *9*, 925–938.

Galvin, S. J., Williams, D. R., & Coletta, N. J. (1996). The spatial grain of motion perception in human peripheral vision. *Vision Research*, *36*, 2283–2295.

Jennings, J. A. M., & Charman, W. N. (1981). Off-axis image quality in the human eye. *Vision Research*, *21*, 445–455.

Jennings, J. A. M., & Charman, W. N. (1997). Analytic approximation of the off-axis modulation transfer function of the eye. *Vision Research*, *37*, 697–704.

Lotmar, W. (1971). Theoretical eye model with aspherics. *Journal of the Optical Society of America*, *61*, 1522–1529.

Lotmar, W., & Lotmar, T. (1974). Peripheral astigmatism in the human eye: experimental data and theoretical model predictions. *Journal of the Optical Society of America*, *64*, 510–513.

Mahajan, V. N. (1991). *Aberration theory made simple*. Washington DC: SPIE Optical Engineering Press.

Millodot, M., & Lamont, A. (1974). Refraction of the periphery of the eye. *Journal of the Optical Society of America*, *64*, 110–111.

Navarro, R., Artal, P., & Williams, D. R. (1993). Modulation transfer of the human eye as a function of retinal eccentricity. *Journal of the Optical Society of America*, *A10*, 201–212.

Pomerantzeff, O., Pankratov, M., Wang, G., & Dufault, P. (1984). Wide-angle optical model of the eye. *American Journal of Optometry and Physiological Optics*, *61*, 166–176.

Rempt, F., Hoogerheide, J., & Hoogenboom, W. P. H. (1971). Peripheral retinoscopy and the skiagram. *Ophthalmologica*, *162*, 1–10.

Röhler, R. (1962). Die abbildungseigenschaften der augenmedien. *Vision Research*, *2*, 391–429.

Santamaría., J., Artal, P., & Bescós, J. (1987). Determination of the point-spread function of human eyes using a hybrid optical-digital method. *Journal of the Optical Society of America*, *A4*, 1109–1114.

Smith, G., & Lu, C. (1991). Peripheral power errors and astigmatism of eyes corrected with intraocular lenses. *Optometry and Vision Science*, *68*, 12–21.

Thibos, L. N. (1987). Calculation of the influence of lateral chromatic aberration on image quality across the visual field. *Journal of the Optical Society of America*, *A4*, 1673–1680.

Thibos, L. N., Still, D. L., & Bradley, A. (1996). Characterization of Spatial Aliasing and Contrast Sensitivity in Peripheral Vision. *Vision Research*, *36*, 249–258.

Wang, Y, Thibos, L. N., & Bradley, A. (1997). Effects of refractive error on detection acuity and resolution acuity in peripheral vision. *Investigations in Ophthalogy and Vision Science*, *74*, 2134–2143.

Wang, Y, & Thibos, L. N. (1997). Oblique (off-axis) astigmatism of the reduced schematic eye with elliptical refractive surface. *Optometry and Vision Science*., *74*, 557–562.

Williams, D. R., Artal, P., Navarro, R., McMahon, M. J., & Brainard, D. H. (1996). Off-axis optical quality and retinal sampling in the human eye. *Vision Research*, *36*, 1103–1114.